JMEPEG
https://doi.org/10.1007/s11665-023-08868-4

1059-9495/$19.00

ORIGINAL RESEARCH ARTICLE

Effect of Synergistic Alloying of Co and Mo on Solidification Microstructure and Properties of NiAl-Based Eutectic High-Entropy Alloy

Jiaxing Feng, Xicong Ye, Haofeng Lei, Junchao Chen, Zhongheng Diao, Guangwei Zhao, Bo Li, and Dong Fang

Submitted: 14 August 2023 / Revised: 30 September 2023 / Accepted: 6 October 2023

NiAl-based alloys possess desirable characteristics such as lightweight, high modulus, and excellent oxidation resistance, making them promising materials for aerospace and other applications. However, the limited room-temperature plasticity of NiAl alloy hinders its manufacturing and practical use. The incorporation of Mo and Co through alloying treatment can significantly enhance the room-temperature plasticity of NiAl-based alloys. A series of eutectic high-entropy alloys, $(NiAl)_{65}V_{20}Cr_{10}Mo_{5-x}Co_x$ (x = 0, 1, 2, 3, 4, and 5), were fabricated through non-consumable vacuum melting. The influence of Co and Mo contents on the microstructure and mechanical properties of these alloys was investigated. The findings indicate that the phase composition of the alloy remains unaffected by the presence of Mo and Co in its content. With an increase in Co content and a decrease in Mo content, the primary B2 phase gradually increases in the alloy, leading to a microstructural transition from complete eutectic structure (x = 0) to hypoeutectic structure ($x > 1$). The strength of the alloy exhibits an initial increase followed by a decrease. At low Co contents, the fracture strength and strain of the alloy experience significant enhancement. $(NiAl)_{65}V_{20}Cr_{10}Mo_3Co_2$ demonstrates superior compressive properties, with its yield strength, fracture strength, and plasticity reaching 1761 MPa, 3009 MPa, and 33.5%, respectively. The changes in the mechanical properties of alloys are primarily attributed to solid solution strengthening, lattice misfit, fine crystal strengthening, and relative variations in phase content.

Keywords microstructure, mechanical property, NiAl-based alloy, synergistic alloying

1. Introduction

Cantor and Yeh (Ref 1, 2) reported a type of alloy with high configurational entropy-high-entropy alloys (HEAs) in 2004, which are composed of equal proportions of five or more major elements. Early high-entropy alloys mainly referred to single-phase structures. Similar to traditional alloys, these materials also faced the challenge of matching strength and ductility. For instance, high-entropy alloys featuring single-phase FCC structures exhibit favorable ductility but limited strength (Ref 3, 4), whereas those with single-phase BCC structures possess high strength yet poor plasticity (Ref 5). Furthermore, element segregation can result in inadequate castability and uneven microstructure distribution within high-entropy alloys (Ref 6-8).

To address the limitations of traditional high-entropy alloys, Lu proposed the concept of eutectic high-entropy alloys (Ref 9), which exhibit low-energy phase boundaries, controllable microstructures, high fracture strength, and excellent creep resistance at elevated temperatures. Additionally, isothermal transformation during solidification (without a temperature range) reduces element segregation and ingot shrinkage in eutectic alloys. Therefore, eutectic high-entropy alloys can complement the advantages and disadvantages of single-phase structures, achieving a balance between fracture strength and ductility for designing and applying strong-plasticity-matched high-entropy alloys with infinite possibilities. Based on the potential high-temperature creep resistance, thermal stability, and anti-softening properties of eutectic high-entropy alloys, researchers have developed various types (Ref 10-16).

NiAl-based alloys exhibit low density, high melting point, excellent thermal conductivity, and exceptional oxidation resistance, rendering them a highly promising material for high-temperature applications (Ref 17, 18). Despite its high strength in the long-term ordered crystal structure of B2 phase, poor ductility at room temperature (Ref 19, 20) severely limits the application of NiAl alloy. In order to enhance the mechanical properties of NiAl, various methods have been employed by researchers to develop a range of NiAl-based alloys and composites (Ref 21-27). Among these approaches, incorporating alloying elements such as V, Cr, and Mo into the NiAl matrix can significantly enhance its plasticity and strength (Ref 28-30).

Jiaxing Feng, Haofeng Lei, Junchao Chen, and **Zhongheng Diao**, College of Mechanical & Power Engineering, China Three Gorges University, Yichang 443002, China; and **Xicong Ye, Guangwei Zhao, Bo Li,** and **Dong Fang**, Hubei Engineering Research Center for Graphite Additive Manufacturing Technology and Equipment, China Three Gorges University, Yichang 443002, China; and College of Mechanical & Power Engineering, China Three Gorges University, Yichang 443002, China. Contact e-mails: yexc@ctgu.edu.cn and zgwhit@126.com.

Published online: 20 October 2023

The concept of eutectic high-entropy alloy also offers a novel design direction for researchers. In the initial stage, the research group incorporated the notion of high-entropy alloy into NiAl-based alloys and devised a new type of $(NiAl)_{65}V_{20}Cr_{10}Mo_5$ eutectic high-entropy alloy based on the infinite solid solution strategy (Ref 31). This alloy exhibits a B2/BCC structure as a eutectic high-entropy alloy. The eutectic layer comprises both the B2 phase and the BCC phase, accompanied by nanometer-sized precipitates in these two phases. Compared to most NiAl-based alloys, this particular alloy demonstrates superior comprehensive mechanical properties. Co is a highly soluble metal in NiAl alloys, and when its content reaches a certain level, it can effectively coordinate the deformation between adjacent grains, thereby achieving superior plasticity (Ref 32). Additionally, Co can reduce the interlamellar spacing between phases in NiAl-based alloys, significantly enhancing their compressive strength (Ref 33). Mo and NiAl can form eutectic alloys, improving the room-temperature plasticity of NiAl-based alloys, and their interlayer spacing is related to Mo content (Ref 34). The CoCrFeNi alloy system has shown that the synergistic alloying of Co and Mo can effectively enhance mechanical properties and achieve a favorable balance between strength and ductility (Ref 35). However, research on the synergistic alloying of Co and Mo in NiAl-based alloys is relatively limited. Therefore, based on the previous research (Ref 23), this study performs Co alloying for $(NiAl)_{65}V_{20}Cr_{10}Mo_5$ and adjusts the Co and Mo content in the eutectic high-entropy alloy of $(NiAl)_{65}V_{20}Cr_{10}Mo_5$, aiming to systematically investigate the influence of synergistic Co and Mo alloying on the microstructure and mechanical properties of $(NiAl)_{65}V_{20}Cr_{10}Mo_5$.

2. Experimental Methods

The $(NiAl)_{65}V_{20}Cr_{10}Mo_{5-x}Co_x$ (x = 0, 1, 2, 3, 4 and 5) eutectic high-entropy alloys were prepared through vacuum arc melting in a high-vacuum argon atmosphere using Ni, Al, V, Mo, Cr and, Co with a purity level exceeding 99.95%. For the sake of convenience, the alloys are denoted as Co-0, Co-1, Co-2, Co-3, Co-4, and Co-5 for brevity. To prevent residual oxygen, titanium is utilized for pre-melting oxygen absorption and each alloy ingot undergoes six rounds of melting and flipping to ensure a uniform composition. Microstructural characterization and mechanical performance testing were conducted by cutting samples (Φ5 mm × 6 mm) from the alloy ingot using wire cutting. The polished samples were analyzed for phase identification from 20° to 90° using the Ultima IV multifunctional x-ray diffractometer (XRD) under Cu-Kα radiation (k = 1.5418 Å). The microstructure of the samples corroded with aqua regia (nitric acid/hydrochloric acid = 1:3 (V%)) was characterized using a scanning electron microscope (SEM) and an energy-dispersive x-ray spectrometer (EDS). The room-temperature compression test was conducted using an electronic universal testing machine (WDW-100E) at a strain rate of 10^{-3} s^{-1}. Three samples were tested for each alloy to determine the average value. To minimize measurement errors, each sample underwent six repetitions of Vickers hardness testing (MH-6L) under a load of 100 N for 10 s.

3. Results and Discussion

3.1 Phase Composition and Microstructure

Figure 1 illustrates the x-ray diffraction patterns of $(NiAl)_{65}V_{20}Cr_{10}Mo_{5-x}Co_x$ (x = 0, 1, 2, 3, 4, and 5) alloys, indicating that Co and Mo variations did not result in new phases; all studied alloys consisted of BCC and B2 phases. The enlarged image of BCC diffraction peaks at 72.5°–77.5° is depicted in Fig. 1(b). With an increase in Co content, the BCC diffraction peak of the alloy shifts toward a higher angle. In accordance with the Bragg equation, the lattice constant of the alloy gradually decreases. The lattice parameters of the B2 phase in the alloy decrease with increasing Co content, as shown in Table 1. Notably, B2 and BCC exhibit similar lattice constants, indicating a lower degree of lattice misfit between the two phases. The formula for calculating lattice misfit is (Ref 36): $\delta = |2(a_1 - a_2)|/(a_1 + a_2)$, where a_1 and a_2 represent the lattice constants of the two phases in the alloy.

Figure 2 displays the BSE microstructure of NiAl-based alloys with varying Co and Mo contents. The Co-0 sample exhibits a typical eutectic structure, where eutectic dendrites consist of alternating thin sheets of BCC and B2 phases that radiate from the center to the boundaries of crystal cells or dendrites. The interior region displays regular lamellar structures with fine layers, while the boundary region exhibits irregular coarse lamellar eutectic structures. This is because the eutectic structure at the grain boundary is influenced by the thermal energy released during solidification from the pre-eutectic cluster, which is a common microstructural characteristic in eutectic high-entropy alloys (Ref 9, 31). From Co-0 to Co-1 alloys, it was observed that the regular interlayer spacing in the eutectic cell increased from 0.45 nm to 0.75 nm, and there was a noticeable coarsening of irregular layers at the eutectic cell boundary with some layer orientations changing. During solidification of the Co-2 alloy, the B2 phase precipitates as the primary crystal while the remaining liquid undergoes eutectic transformation near it to form regular lamellar structures that extend outward to the boundary where they become irregular lamellar eutectic structures. With the further increase in Co addition, the distribution of the primary B2 phase gradually increases in Co-3, Co-4, and Co-5. Additionally, there is a sequential enlargement observed in

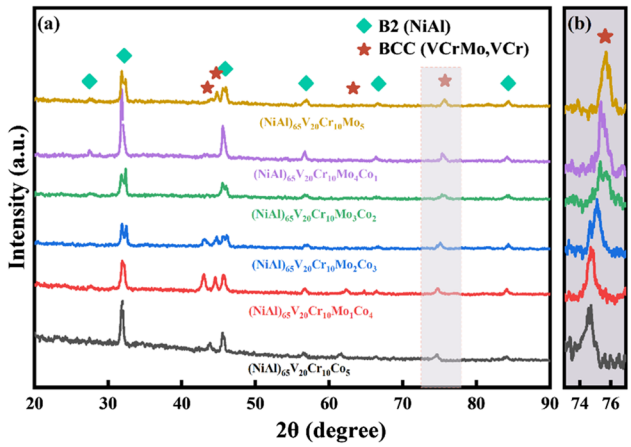

Fig. 1 (a) XRD patterns of $(NiAl)_{65}V_{20}Cr_{10}Mo_{5-x}Co_x$ (x = 0, 1, 2, 3, 4, and 5) alloys, (b) 74°–76° enlarge image

Table 1 Lattice parameters and lattice misfit of $(NiAl)_{65}V_{20}Cr_{10}Mo_{5-x}Co_x$ alloys

Alloys	Lattice parameters, Å		Lattice misfit
	BCC	B2	|δ|
Co-0	2.959	2.886	0.0249
Co-1	2.931	2.881	0.0172
Co-2	2.904	2.880	0.0083
Co-3	2.893	2.877	0.0055
Co-4	2.887	2.877	0.0034
Co-5	2.863	2.875	0.0042

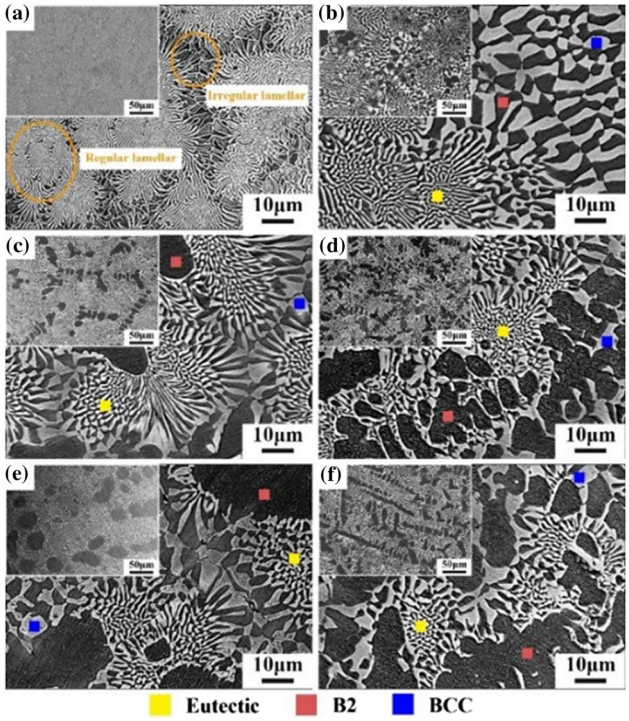

Fig. 2 BSE-SEM images of $(NiAl)_{65}V_{20}Cr_{10}Mo_{5-x}Co_x$: (a) Co-0, (b) Co-1, (c) Co-2, (d) Co-3, (e) Co-4, (f) Co-5

both regular and irregular interlayer spacing. To visually demonstrate these changes in the primary phase and regular interlayer spacing, the measurement results are presented in Table 3. The study revealed that both Co and Mo have the ability to refine the eutectic interlamellar spacing in NiAl-based alloys (Ref 33, 34). However, an increase in Co content and a decrease in Mo content resulted in larger regular and irregular interlamellar spacings. Therefore, it can be concluded that Mo has a stronger impact on refining the lamellar structure of NiAl-based alloys compared to Co.

Based on the point energy spectrum results presented in Table 2, it can be inferred that the gray-white BCC phase is enriched with V, Cr, and Mo (with $x = 5$ being rich in V and Cr), while the black B2 phase exhibits a high concentration of Ni and Al. The comparable Co content observed in both phases suggests that Co has similar solubility characteristics in NiAl and VCrMo. Meanwhile, as the Co content increases, the overall VCrMo content forming BCC solid solution decreases, thereby facilitating the transformation of eutectic structure to hypoeutectic structure, which is in line with the findings from BSE analysis. With the increase in Co, the concentrations of Ni and Al in the NiAl phase gradually decrease, suggesting that Co may occupy either Ni or Al sites (Ref 37). The position preference of Co in NiAl has been extensively investigated by numerous researchers (Ref 38-40), revealing a tendency for Co to replace the position occupied by Ni. The data presented in Table 2 also demonstrate the limited solubility of Mo in the B2 phase, a phenomenon that has been observed repeatedly in NiAl-Cr(Mo) alloys (Ref 13, 23, 26). This further confirms the reduction of Mo content and its role in promoting the transformation from eutectic to hypoeutectic alloy (with the B2 phase as the primary crystal).

In order to select appropriate elements from a wide range of options and determine the proportions of each element, thus achieving a suitable composition for preparing high-entropy alloy systems with exceptional performance, researchers have summarized and proposed structural formation rules and criteria for high-entropy alloys based on thermodynamic parameters, valence electron concentration (VEC), and atomic size mismatch (δ_r). The calculation formula is as follows:

$$\mathrm{VEC} = \sum_{i=1}^{n} c_i (\mathrm{VEC})_i \quad \text{(Eq 1)}$$

$$\Omega = T_m \Delta S / |\Delta H|, \quad T_m = \sum_{i=1}^{n} c_i (T_m)_i \quad \text{(Eq 2)}$$

$$\Delta S_{\mathrm{mix}} = -R \sum_{i=1}^{n} (c_i \ln c_i) \quad \text{(Eq 3)}$$

$$\Delta H_{\mathrm{mix}} = \sum_{i=1, i \neq j}^{n} 4 \Delta H_{ij} c_i c_j \quad \text{(Eq 4)}$$

$$\delta_r = \sqrt{\sum_{i=1}^{n} c_i \left(1 - \frac{r_i}{\overline{r}}\right)^2}, \quad \overline{r} = \sum_{i=1}^{n} c_i r_i \quad \text{(Eq 5)}$$

In the formula, R is the gas constant, n is the number of atoms, $\overline{r}$ is the average atomic radius, c_i, r_i, ΔH_{ij}, $(T_m)_i$ and $(\mathrm{VEC})_i$, respectively, represent atomic percentages, atomic radii, mixed enthalpies of elements i and j, melting points and valence electrons.

Yang (Ref 41) employed the Ω parameter to distinguish between the solid solution phase (SS) and intermetallic compound phase (IM), when $1.1 \leq \Omega \leq 10$ and $3.6\% \leq \delta_r \leq 6.6\%$, the alloy comprises both intermetallic compounds and a solid solution phase. However, in this study, the Ω value falls outside this range, possibly due to an excessively negative mixing enthalpy within the alloy composition. As per the calculation formula, a higher absolute value of mixing enthalpy leads to a smaller computed value for Ω. The thermodynamic parameters of the eutectic high-entropy alloy system, as studied by Li et al. (Ref 42), indicate that when the entropy of mixing is low ($\Delta S_{\mathrm{mix}} < 12$ J/k mol) and the mixing enthalpy is very negative (-20 kJ/mol $< \Delta H_{\mathrm{mix}} < -14$ kJ/mol), the constituent phases of the eutectic high-entropy alloy tend to form a B2 ordered structure. However, this criterion cannot determine whether a BCC solid solution exists in the alloy. Guo (Ref 43) proposed that the formation of a BCC structure solid solution in the alloy occurs when VEC ≤ 6.87. Since the criterion

Table 2 Chemical composition of BCC and B2 phase in the $(NiAl)_{65}V_{20}Cr_{10}Mo_{5-x}Co_x$ alloys

Alloys	Region	Ni, at.%	Al, at.%	V, at.%	Cr, at.%	Mo, at.%	Co, at.%
Co-0	Eutectic	32.43	31.17	20.14	10.43	5.82	…
	BCC	15.26	14.90	40.33	21.12	8.38	…
	B2	43.39	41.76	10.35	4.15	0.48	…
Co-1	Eutectic	32.21	31.82	20.42	9.82	4.64	1.09
	BCC	13.04	16.04	40.61	20.92	8.36	1.03
	B2	42.96	41.97	9.35	4.23	0.36	1.13
Co-2	Eutectic	32.41	32.26	19.52	9.94	4.00	1.86
	BCC	13.79	15.36	40.9	20.21	7.82	1.92
	B2	42.35	41.54	9.93	3.87	0.49	1.82
Co-3	Eutectic	32.41	32.25	19.67	9.87	2.74	3.07
	BCC	13.76	15.05	42.01	22.22	3.87	3.09
	B2	41.91	39.90	10.35	4.26	0.52	3.06
Co-4	Eutectic	32.01	32.30	19.74	10.35	1.45	4.15
	BCC	14.11	14.63	42.69	21.8	2.73	4.04
	B2	41.37	39.13	10.62	4.43	0.38	4.07
Co-5	Eutectic	32.53	32.48	19.92	10.09	…	4.98
	BCC	15.89	16.13	40.51	22.43	…	5.04
	B2	40.88	39.30	10.69	4.22	…	4.91

classifies the B2 phase as a BCC solid solution, it can be applied for phase prediction of the alloy in this study.

3.2 Room-Temperature Mechanical Properties

Figure 3 illustrates the variation in hardness of $(NiAl)_{65}V_{20}Cr_{10}Mo_{5-x}Co_x$ alloy with varying Co content. By combining Table 3 and Fig. 3, it is evident that the addition of Co promotes an increase in the B2 phase within the alloy and also leads to a rise in the B2 phase hardness as Co content increases, with Co-5 hardness reaching the maximum value of 715HV. According to the findings of researchers (Ref 13, 23, 26) and the point energy spectrum results presented in Table 2, it is evident that the solid solubility of Mo in NiAl exhibits a relatively small magnitude. Thereby, the influence of Mo reduction within the alloy system on lattice distortion in NiAl can be considered practically negligible. The significant difference in atomic radius between Co and Al results in the B2 phase hardness being strengthened by the solid solution strengthening effect of Co. As the B2 phase has higher hardness compared to the eutectic (BCC + B2 phase) structure, it acts as a reinforcing component within the alloy. Therefore, an increase in B2 phase content is expected to correspondingly enhance alloy strength.

The strength of the alloy, however, does not exhibit a consistently increasing trend overall; it initially rises before subsequently declining. The engineering stress–strain curves for $(NiAl)_{65}V_{20}Cr_{10}Mo_{5-x}Co_x$ (x = 0, 1, 2, 3, 4, and 5) eutectic high-entropy alloys are presented in Fig. 4. Co-0 exhibits a yield strength of 1470 MPa, fracture strength of 2410 MPa, and plasticity of 24.5%. The compressive strength of the alloy initially increases significantly with an increase in Co content, reaching its maximum value at Co-2 with a yield strength of 1761.9 MPa and a fracture strength of 3009.9 MPa, while exhibiting plasticity of 33.5%. As the Co content further increases, there is a decline observed in the overall mechanical properties of the alloy. Please refer to Table 4 for specific data. However, overall, through the synergistic alloying effect of Mo and Co, the comprehensive mechanical properties of NiAl-based alloys are superior to those of single alloying using Mo or Co.

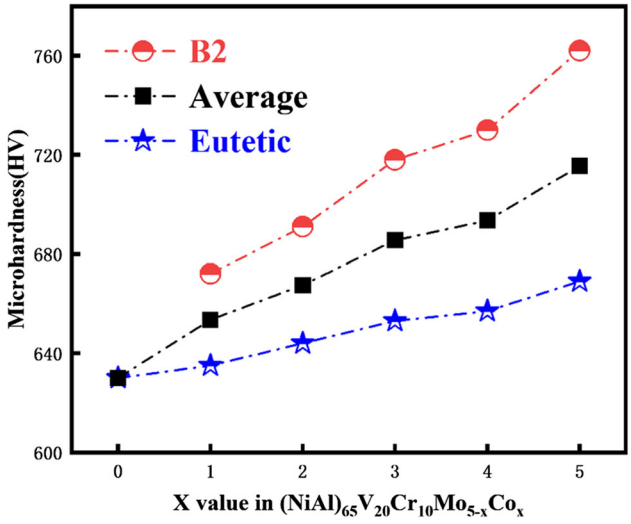

Fig. 3 Relationship between Co addition and microhardness in $(NiAl)_{65}V_{20}Cr_{10}Mo_{5-x}Co_x$

The mechanical properties of alloys can be analyzed from multiple perspectives. (a) Lattice misfit. The increase in Co content and a decrease in Mo content, result in a variation of the lattice misfit between BCC and B2 phases, which initially decreases and then increases. This reduction in lattice misfit contributes to the alleviation of lattice strain and strain energy, thereby enhancing the structural stability of the alloy and improving the strength and plasticity of the alloy (Ref 44, 45). (b) Solid solution strengthening. Compared to occupying the lattice sites of Al in the B2 phase, Co occupying the Ni sublattice is more likely to induce vacancy formation. Under the dual effects of replacement defects and vacancy defects, the alloy undergoes significant hardening after lattice distortion (Ref 46). This increases the dislocation density and strength of the alloy while decreasing its plasticity. (c) Grain refinement. In

Table 3 Phase volume fraction and lamellar spacing in $(NiAl)_{65}V_{20}Cr_{10}Mo_{5-x}Co_x$

Alloys	Co-0	Co-1	Co-2	Co-3	Co-4	Co-5
B2 phase (V%)	50.4	53.7	55.4	57.1	59.0	61.4
BCC pahse (V%)	49.6	46.3	44.6	42.9	41.0	38.6
Lamellar spacing (μm)	0.45	0.75	0.81	0.99	1.34	1.49

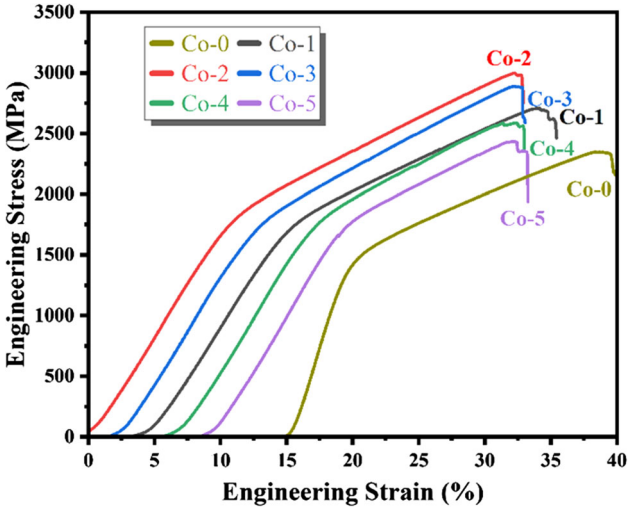

Fig. 4 Compressive stress–strain curve of $(NiAl)_{65}V_{20}Cr_{10}Mo_{5-x}Co_x$ at room temperature

Table 4 Calculation results of physical parameters of $(NiAl)_{65}V_{20}Cr_{10}Mo_{5-x}Co_x$ alloys

HEAs	$\Delta\delta_r$, %	VEC	ΔH_{mix}, kJ/mol	ΔS_{mix}, J/k mol	Ω
Co-0	5.92	6.13	− 18.82	11.51	0.86
Co-1	5.94	6.16	− 19.04	11.72	0.85
Co-2	5.97	6.19	− 19.26	11.79	0.84
Co-3	6.00	6.22	− 19.48	11.79	0.82
Co-4	6.03	6.25	− 19.69	11.72	0.80
Co-5	6.06	6.28	− 19.91	11.51	0.77

general, the refinement of grain size can enhance the strength and ductility of alloys. This is due to an inverse relationship between interlayer spacing size and volume fraction of grain boundaries, indicating that smaller grains increase interfacial anti-slip ability near these boundaries (Ref 47, 48). However, the addition of Co leads to a gradual increase in eutectic cluster interlayer spacing and a decrease in anti-slip ability at grain boundaries, ultimately weakening the alloys' strengthening effect. (d) B2 phase change. As a strengthening phase in the alloy system, the compressive strength of the alloy increases significantly with the increase in the primary B2 phase from Co-0 to Co-2. However, when the Co content exceeds 2 at.%, the compressive properties of the alloy begin to decline due to the high strength and intrinsic low plasticity of the B2 phase. Similarly, the hardness and strength of certain eutectic high-entropy alloys increase with an increase in primary phase content after the alloy transforms from eutectic to hypoeutectic,

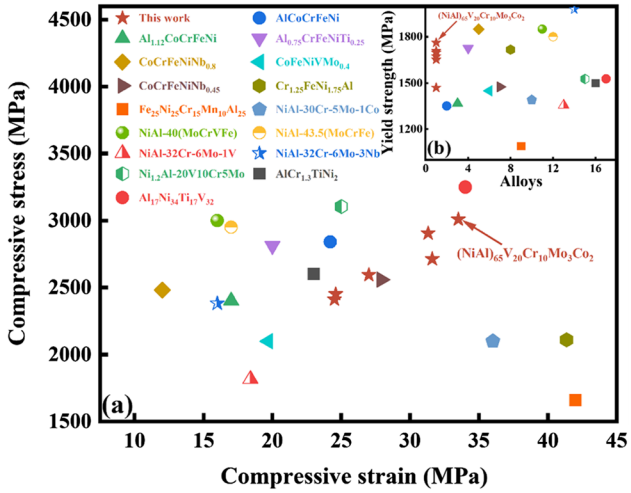

Fig. 5 Compressive properties of NiAl-based HEAs and HEAs containing Co: (a) compressive stress–strain diagram and (b) yield strength

while the fracture strain decreases (Ref 49, 50). The aforementioned factors contribute to the optimal comprehensive mechanical properties of Co-2 alloy.

The compressive performance of typical NiAl-based high-entropy alloys and Co-containing high-entropy alloys (Ref 13-15, 23, 33, 49-58) is illustrated in Fig. 5. Both $Ni_{1.2}Al$-20V10Cr5Mo (Ref 49) and NiAl-Mo10Cr10V10Fe10 (Ref 15) possess a BCC + B2 structure. Although their strength is marginally higher than that of Co-2 alloy, Co-2 exhibits superior fracture strain which is approximately three times greater than the former two alloys. While the yield strength of $CoCrFeNiNb_{0.8}$ (Ref 53), NiAl-Mo10Cr10V10Fe10 (Ref 15), and NiAl-32Cr-6Mo-3Nb (Ref 58) exceeds 1800 MPa, Co-1, Co-2, and Co-3 exhibit higher fracture strength and fracture strain. On the other hand, $Cr_{1.25}FeNi_{1.75}A$ l (Ref 56) and NiAl-30Cr-5Mo-1Co (Ref 33) demonstrate better plasticity but lower fracture strength compared to Co-2 by nearly 900 MPa. Furthermore, AlCoCrFeNi (Ref 54) alloy has added a large amount of Co as the main element, and adding a small amount of Co in this article can achieve the combination of high strength and plasticity, which means that the alloys studied in this article is a new type of structural material with broad application prospects.

4. Conclusion

The incorporation of Co into NiAl-based eutectic high-entropy alloys was carried out to achieve synergistic alloying of Co and Mo in the NiAl-based alloys. A series of eutectic high-

entropy alloys were prepared using vacuum arc melting and water-cooled copper crucible rapid solidification. The influence of synergistic alloying on the microstructure and mechanical properties of NiAl-based alloys was investigated, and the specific conclusions are as follows:

1. The relative changes in Co and Mo content did not affect the phase composition of $(NiAl)_{65}V_{20}Cr_{10}Mo_{5-x}Co_x$ eutectic high-entropy alloys, which consist of both BCC and B2 phases. Among them, Co is uniformly distributed in both B2 and BCC phases, Mo primarily forms the BCC solid solution with V and Cr, and Mo is almost insoluble in the B2 phase, which is rich in Ni and Al elements.
2. With an increase in Co content and a decrease in Mo content, the microstructure of the alloy transitions from eutectic ($x = 0$) to hypoeutectic ($x > 0$). This transformation is primarily attributed to the reduction of Mo, which is a forming element of BCC phase. The addition of Co results in an increase in regular and irregular interlayer spacing within eutectic clusters, indicating that Mo has a stronger refining effect on eutectic layers than Co.
3. The synergistic alloying of Co and Mo exhibits superior effects on the comprehensive mechanical properties of the alloy compared to individual alloying with either Co or Mo. With increasing Co content and decreasing Mo content, the yield strength, fracture strength, and compressive strain of the alloy first increase and then decrease due to a combination of solid solution strengthening, lattice mismatch, B2 phase change, and changes in lamellar spacing. The Co-2 alloy exhibits the best comprehensive mechanical properties with yield strength, fracture strength, and compressive strain reaching 1761 MPa, 3009 MPa, and 33.5%, respectively.

Acknowledgments

The research was financially supported by Major Technological Innovation project of Hubei science and Technology Department (2019AAA164).

Author Contributions

JF: Conceptualization, Investigation, Validation, Writing—Original Draft, Writing—Review and Editing; XY: Methodology, Writing—Review and Editing, Resources; HL: Investigation, Visualization; JC: Investigation; ZD: Investigation; GZ: Writing—Review and Editing; BL: Formal analysis; DF: Formal analysis.

Date and code availability

Data will be made available on request.

Conflict of interest

The authors declare that they have no known competing financial interests or personal relationships that could have appeared to influence the work reported in this paper.

References

1. J.W. Yeh, S.K. Chen, S.J. Lin, J.Y. Gan, T.S. Chin, T.T. Shun, C.H. Tsau, and S.Y. Chang, Nanostructured High-Entropy Alloys with Multiple Principal Elements: Novel Alloy Design Concepts and Outcomes, *Adv. Eng. Mater.*, 2004, **6**(5), p 299–303
2. B. Cantor, I.T.H. Chang, P. Knight, and A.J.B. Vincent, Microstructural Development in Equiatomic Multicomponent Alloys, *Mater. Sci. Eng. A*, 2004, **375–377**, p 213–218
3. J. Joseph, N. Stanford, P. Hodgson, and D.M. Fabijanic, Understanding the mechanical Behaviour and the Large Strength/Ductility Differences Between FCC and BCC AlxCoCrFeNi High Entropy Alloys, *J. Alloys Compd.*, 2017, **726**, p 885–895
4. F. Otto, A. Dlouhý, C. Somsen, H. Bei, G. Eggeler, and E.P. George, The Influences of Temperature and Microstructure on the Tensile Properties of a CoCrFeMnNi High-Entropy Alloy, *Acta Mater.*, 2013, **61**(15), p 5743–5755
5. O. Senkov, J. Scott, S. Senkova, D. Miracle, and C. Woodward, Microstructure and Room Temperature Properties of a High-Entropy TaNbHfZrTi Alloy, *J. Alloys Compd.*, 2011, **509**(20), p 6043–6048
6. X. Gao, L. Wang, N. Guo, L. Luo, G. Zhu, C. Shi, Y. Su, and J. Guo, Microstructure Characteristics and Mechanical Properties of $Hf_{0.5}Mo_{0.5}NbTiZr$ Refractory High Entropy Alloy with Cr Addition, *Int. J. Refract. Met. Hard Mater.*, 2021, **95**, p 105405
7. Q. Li, H. Zhang, D. Li, Z. Chen, and Z. Qi, The Effect of Configurational Entropy on Mechanical Properties of Single BCC Structural Refractory High-Entropy Alloys Systems, *Int. J. Refract Metal Hard Mater.*, 2020, **93**, 105370
8. M.G.M. Poletti, C.M. Fiore, G. Goodall, and R. Battezzati, Refractory High Entropy Alloys: CrMoNbTiVWZr and Al(x)Cr(y)NbMoTiV(z)Zry(x = 0,0.6;y = 0.3,z = 0,0.6), *Int. J. Refract. Met. Hard Mater.*, 2018, **76**, p 25
9. Y. Lu, Y. Dong, S. Guo, L. Jiang, H. Kang, T. Wang, B. Wen, Z. Wang, J. Jie, Z. Cao, H. Ruan, and T. Li, A promising new class of high-temperature alloys: eutectic high-entropy alloys, *Sci. Rep.*, 2014, **4**, p 6200
10. M. Abdullah, M. Mukarram, T.B. Yaqub, F. Fernandes, and K. Yaqoob, Development of eutectic high entropy alloy by addition of W to CoCrFeNi HEA, *Int. J. Refract Metal Hard Mater.*, 2023, **115**, 106300
11. H. Jiang, D. Qiao, Y. Lu, Z. Ren, Z. Cao, T. Wang, and T. Li, Direct solidification of bulk ultrafine-microstructure eutectic high-entropy alloys with outstanding thermal stability, *Scr. Mater.*, 2019, **165**, p 145–149
12. Z. Li, C. Jing, Y. Feng, Z. Wu, T. Lin, and J. Zhao, Microstructure evolution and properties of laser cladding Nb containing eutectic high entropy alloys, *Int. J. Refract Metal Hard Mater.*, 2023, **110**, 105992
13. M. Wang, Y. Lu, G. Zhang, H. Cui, D. Xu, N. Wei, and T. Li, A novel high-entropy alloy composite coating with core-shell structures prepared by plasma cladding, *Scr. Mater.*, 2021, **204**, 114132
14. M. Wang, Y. Lu, J. Lan, T. Wang, C. Zhang, Z. Cao, T. Li, and P.K. Liaw, Lightweight, ultrastrong and high thermal-stable eutectic high-entropy alloys for elevated-temperature applications, *Acta Mater.*, 2023, **248**, 118806
15. L. Wang, C. Yao, J. Shen, Y. Zhang, G. Liu, X. Wu, and G. Zhang, A new method to design eutectic high-entropy alloys by determining the formation of single-phase solid solution and calculating solidification paths, *Mater. Sci. Eng. A*, 2022, **830**, 142325
16. L. Wang, X. Wu, C. Yao, J. Shen, Y. Zhang, Y. Ge, and G. Zhang, Microstructural Stability of As-Cast and Directionally Solidified $AlCoCrFeNi_{2.1}$ Eutectic High-Entropy Alloys at Elevated Temperatures, *Metall. Mater. Trans. A*, 2020, **51**, p 5781–5789
17. J. Zhou and J. Guo, Effect of Ag Alloying on Microstructure, Mechanical and Electrical Properties of NiAl Intermetallic Compound, *Mater. Sci. Eng. A*, 2003, **339**(1–2), p 166–174
18. X.-H. Du, C. Gao, B.-L. Wu, Y.-H. Zhao, and J.-J. Wang, Enhanced Compression Ductility of Stoichiometric NiAl at Room Temperature by Y and Cu Co-addition, *Int. J. Miner. Metall. Mater.*, 2012, **19**, p 348–353
19. B. Han, Y. Ma, H. Peng, L. Zheng, and H. Guo, Effect of Mo, Ta, and Re on High-Temperature Oxidation Behavior of Minor Hf Doped β-NiAl Alloy, *Corros. Sci.*, 2016, **102**, p 222–232
20. L. Sheng, F. Yang, J. Guo, T. Xi, and H. Ye, Investigation on NiAl–TiC–Al_2O_3 Composite Prepared by Self-Propagation High Tempera-

ture Synthesis with Hot Extrusion, *Compos. B Eng.*, 2013, **45**(1), p 785–791
21. J.-M. Yang, S. Jeng, K. Bain, and R. Amato, Microstructure and Mechanical Behavior of In-Situ Directional Solidified NiAl/Cr (Mo) Eutectic Composite, *Acta Mater.*, 1997, **45**(1), p 295–308
22. L. Wang, Y. Su, C. Yao, Y. Huang, J. Shen, Y. Zhang, G. Liu, P. Zhao, and G. Zhang, Microstructure and Mechanical Property of Novel NiAl-Based Hypoeutectic/Eutectic/Hypereutectic High-Entropy Alloy, *Intermetallics*, 2022, **143**, 107476
23. Z. Shang, Q. Zhang, J. Shen, H. Bai, H. Liang, L. Zhong, and Y. Xu, Effects of V Addition on the Solidification Microstructures and Room Temperature Compression Properties of NiAl–Cr (Mo) Hypereutectic Alloy, *Vacuum*, 2020, **179**, 109507
24. L. Wang, L. Gao, J. Shen, Y. Zhang, G. Liu, P. Zhao, and G. Zhang, Eutectic Composition Design, Microstructure, and Room Temperature Mechanical Property of NiAl-Cr-Ta Three-Phase Alloy, *Metall. Mater. Trans. A*, 2022, **53**, p 254
25. D. Wang, H. Ning, B. Wang, G. Liu, and S. Yuan, Fabrication of a NiAl–Cr(Mo) Eutectic Alloy with Network Microstructure for High-Temperature Strengthening, *Mater. Sci. Eng. A*, 2022, **835**, p 142628
26. H. Ning, D. Wang, B. Wang, and G. Liu, Investigations on the NiAl–Cr (Mo) Eutectic Alloy with Optimized Microstructure and Improved Room-Temperature Compressive Properties, *Mater. Sci. Eng. A*, 2021, **813**, 141138
27. L. Wang, C. Yao, J. Shen, Y. Zhang, T. Wang, H. Xu, L. Gao, and G. Zhang, Microstructures and Compressive Properties of NiAl-Cr (Mo) and NiAl-Cr Eutectic Alloys with Different Fe Contents, *Mater. Sci. Eng. A*, 2019, **744**, p 593–603
28. S. Milenkovic and R. Caram, Mechanical Properties and Fracture Behavior of Directionally Solidified NiAl-V Eutectic Composites, *Metall. Mater. Trans. A*, 2015, **46**(2), p 557–565
29. X. Du, J. Guo, and B. Zhou, Superplastic Behavior in Pseudo-Eutectic NiAl–9Mo Alloy, *Mater. Lett.*, 2002, **52**(6), p 442–447
30. M. Kellner, J. Hötzer, E. Schoof, and B. Nestler, Phase-Field Study of Eutectic Colony Formation in NiAl-34Cr, *Acta Mater.*, 2020, **182**, p 267–277
31. X. Ye, J. Xiong, X. Wu, C. Liu, D. Xu, W. Zhang, D. Fang, and B. Li, A New Infinite Solid Solution Strategy to Design Eutectic High Entropy Alloys with B2 and BCC Structure, *Scr. Mater.*, 2021, **199**, 113886
32. J.D. Cotton, R.D. Noebe, and M.J. Kaufman, The Effects of Chromium on NiAl Intermetallic Alloys: Part I. Microstructures and Mechanical Properties, *Intermetallics*, 1993, **1**(1), p 3–20
33. D. Wang, Y. Liang, H. Ning, and B. Wang, Effects of Zr and Co on the Microstructure and Mechanical Properties of NiAl-Based Alloys, *J. Alloys Compd.*, 2021, **883**, 160815
34. D. Johnson, X. Chen, B. Oliver, R.D. Noebe, and J. Whittenberger, Processing and Mechanical Properties of In-Situ Composites from the NiAlCr and the NiAl (Cr, Mo) Eutectic Systems, *Intermetallics*, 1995, **3**(2), p 99–113
35. X. Ye, H. Lei, G. Zhao, J. Feng, J. Chen, B. Li, D. Fang, and N. Gao, Design of Synergistic Alloying CoCrFeNi Eutectic High Entropy Alloy Based on Infinite Solid Solution, *Mater. Lett.*, 2023, **343**, 134395
36. Z. Ma, Y.L. Pei, L. Luo, L. Qin, S.S. Li, and S.K. Gong, Partitioning Behavior and Lattice Misfit of γ/γ' Phases in Ni-Based Superalloys with Different Mo Additions, *Rare Met.*, 2021, **40**, p 920–927
37. J. Guo, W. Ren, and J. Zhou, Progress in Research on Alloying Effects in NiAl Intermetallic Alloys, *Acta Metall. Sin. Chin. Ed.*, 2002, **38**(6), p 667–672
38. Y. Hao, R. Yang, Y. Song, Y. Cui, D. Li, and M. Niinomi, Concentration of Point Defects and Site Occupancy Behavior in Ternary NiAl Alloys, *Mater. Sci. Eng. A*, 2004, **365**(1–2), p 85–89
39. C. Jiang, Site Preference of Transition-Metal Elements in B2 NiAl: A Comprehensive Study, *Acta Mater.*, 2007, **55**(14), p 4799–4806
40. Y. Cao, P. Zhu, J. Zhu, and Y. Liu, First-Principles Study of NiAl Alloyed with Co, *Comput. Mater. Sci.*, 2016, **111**, p 34–40
41. X. Yang and Y. Zhang, Prediction of High-Entropy Stabilized Solid-Solution in Multi-component Alloys, *Mater. Chem. Phys.*, 2012, **132**(2–3), p 233–238
42. L. Yahao, T. Yu, Y. Yicong, L. Shun, W. Hong, L. Xiyue, Z. Li'an, W. Zhen, and B. Shuxin, Basic Thermodynamic Research of Eutectic High Entropy Alloys Formation, *Rare Metal Mater. Eng.*, 2021, **50**(5), p 1635–1640
43. S. Guo, C. Ng, J. Lu, and C. Liu, Effect of Valence Electron Concentration on Stability of fcc or bcc Phase in High Entropy Alloys, *J. Appl. Phys.*, 2011, **109**(10), 103505
44. P. Nielaba, P. Fratzl, and J.L. Lebowitz, Growth of Ordered Domains in a Computer Model Alloy with Lattice Misfit, *J. Stat. Phys.*, 1999, **95**(1), p 23–43
45. X.J. Zhang, C.J. Wang, and H. Harada, The Effect of Lattice Misfit on the Dislocation Motion in Superalloys During High-Temperature Low-Stress Creep, *Acta Mater.*, 2005, **53**(17), p 4623–4633
46. R.L. Fleischer, D.M. Dimiduk, and H.A. Lipsitt, Intermetallic Compounds for Strong High-Temperature Materials: Status and Potential, *Annu. Rev. Mater. Res.*, 1989, **19**(1), p 231–263
47. L. Yu, X. Ye, D. Fang, M. Liu, H. Guo, S. Wang, G. Zhao, B. Li, and H. Wu, Precise Design Strategy of FeNiCrMo Eutectic High-Entropy Alloys, *J. Market. Res.*, 2022, **21**, p 3207–3219
48. D. Wu, J. Zhang, J. Huang, H. Bei, and T.-G. Nieh, Grain-Boundary Strengthening in Nanocrystalline Chromium and the Hall-Petch Coefficient of Body-Centered Cubic Metals, *Scr. Mater.*, 2013, **68**(2), p 118–121
49. X. Ye, J. Feng, H. Lei, X. Wu, D. Fang, G. Zhao, and B. Li, Effect of Ni/Al Ratio on Solidification Structure and Properties of NiAl-Based Multi-principal Element Alloy, *J. Mater. Eng. Perform.*, 2023, **25**, p 1–12
50. L. Jiang, Z. Cao, J. Jie, J. Zhang, Y. Lu, T. Wang, and T. Li, Effect of Mo and Ni Elements on Microstructure Evolution and Mechanical Properties of the CoFeNixVMoy High Entropy Alloys, *J. Alloys Compd.*, 2015, **649**, p 585–590
51. R. Gawel, Ł Rogal, and J. Dąbek, Behaviour of Nickel-Rich Non-Equimolar High Entropy Alloys in High-Temperature Oxidizing Conditions, *Mater. Trans.*, 2022, **63**(4), p 442–449
52. H. Jiang, L. Jiang, D. Qiao, Y. Lu, T. Wang, Z. Cao, and T. Li, Effect of Niobium on Microstructure and Properties of the CoCrFeNbxNi High Entropy Alloys, *J. Mater. Sci. Technol.*, 2017, **33**(7), p 712–717
53. F. He, Z. Wang, P. Cheng, Q. Wang, J. Li, Y. Dang, J. Wang, and C.T. Liu, Designing Eutectic High Entropy Alloys of CoCrFeNiNb x, *J. Alloys Compd.*, 2016, **656**, p 284–289
54. L. Cao, X. Wang, Y. Wang, L. Zhang, Y. Yang, F. Liu, and Y. Cui, Microstructural Evolution, Phase Formation and Mechanical Properties of Multi-component AlCoCrFeNix Alloys, *Appl. Phys. A*, 2019, **125**(10), p 1–11
55. S. Liu, M. Gao, P. Liaw, and Y. Zhang, Microstructures and Mechanical Properties of $AlxCrFeNiTi_{0.25}$ Alloys, *J. Alloys Compd.*, 2015, **619**, p 610–615
56. W. Zhang, X. Ye, D. Xu, C. Liu, D. Fang, and B. Li, Microstructures and Properties of CrxFeNi (3–x) Al High-Entropy Alloys, *Appl. Phys. A*, 2022, **128**(1), p 1–9
57. X. Ye, W. Xu, Z. Li, D. Xu, W. Zhang, B. Li, and D. Fang, Microstructures and Mechanical Properties of FeNiCrMnAl High-Entropy Alloys, *J. Mater. Eng. Perform.*, 2022, **31**(10), p 7820–7829
58. Z. Shang, Q. Zhang, J. Shen, H. Bai, and Y. Xu, Effects of Nb/Ti Additions and Heat Treatment on the Microstructure Evolution and Hardness of As-Cast and Directionally Solidified NiAl-Cr(Mo) Alloy, *J. Mater. Res. Technol.*, 2020, **10**, p 745